Performance Analysis of NOMA-Based Land Mobile Satellite Networks

Xiaojuan Yan *Student Member, IEEE*, Hailin Xiao, *Member, IEEE*, Cheng-Xiang Wang, *Fellow, IEEE*, Kang An, Anthony Theodore Chronopoulos, *Senior Member, IEEE*, and Gan Zheng, *Senior Member, IEEE*

***Abstract*—Non-orthogonal multiple access (NOMA) scheme, which has the ability to superpose information in the power domain and serve multiple users on the same time/frequency resource, is regarded as an effective solution to increase transmit rate and fairness. In this paper, we introduce the NOMA scheme in a downlink land mobile satellite (LMS) network and present a comprehensive performance analysis for the considered system. Specifically, we first obtain the power allocation coefficients by maximizing the sum rate while meeting the predefined target rates of each NOMA user. Then, we derive the theoretical expressions for the ergodic capacity and the energy efficiency (EE) of the considered system. Moreover, the outage probability (OP) and average symbol error rate (ASER) performances of NOMA users are derived analytically. To gain further insights, we derive the asymptotic OP at the high signal-to-noise ratio (SNR) regime to characterize the diversity orders and coding gains of NOMA users. Finally, simulation results are provided to validate the theoretical analysis as well as the superiority of employing the NOMA scheme in the LMS system, and show the impact of key parameters such as fading configurations and user selection strategy on the performance of NOMA users.**

Index Terms—**Land mobile satellite network, non-orthogonal multiple access, ergodic capacity, energy efficiency, outage probability, average symbol error rate.**

I. Introduction

Due to the inherent nature of providing vast coverage and economic service in rural areas, land mobile satellite (LMS) networks have received considerable attention in broadcasting, emergency service, and navigation. However, the increasingly growing number of applications and services of satellite communication is rapidly exhausting the limited spectral resources. In this regard, new technique such as the cognitive radio (CR) technology has been introduced in satellite communications, and therefore an important network architecture, referred to as cognitive satellite-terrestrial network [1], has been proposed to enhance spectrum efficiency.

In a cognitive network, a terrestrial network can act as a cognitive/primary system and share the frequency band which is licensed to a satellite/terrestrial network, if the interference caused by the cognitive network is under an interference constraint [2]. Until now, several works have been done to investigate the performance measures of the cognitive satellite-terrestrial network in diverse scenarios, such as outage probability (OP) [3] and effective capacity [4] in single antenna environment. An extension work of [3] to a multi-antenna scenario with beamforming scheme was studied in [5]. Moreover, some studies investigated performance of the cognitive network from the perspective of secure transmission with various targets, i.e., the authors in [6] proposed a joint beamforming scheme to maximize the secrecy rate for the satellite user, while the work in [7] proposed two beamforming schemes to maximize the transmission rate of a terrestrial user. Although the cognitive network can enhance spectrum efficiency of a licensed system, the co-channel interference (CCI) inevitably caused by a cognitive network is the major challenge to improve the performance for a licensed user.

Furthermore, the performance of satellite user can be significantly degraded by a masking effect, i.e., poor elevation angle, fog, or obstacles and therefore a line-of-sight (LoS) link between the LMS and a user is seriously blocked. To address this issue, hybrid satellite-terrestrial relay networks (HSTRNs), in which a relaying technique is adopted to achieve the benefit of spatial diversity, has been proposed in [8] as an effective way to improve the reliability of satellite communications. In recent years, many efforts have been devoted on the HSTRNs from various performance metrics, i.e., average symbol error rate (ASER) was investigated in [9] and [10] with a deteriorated LoS link and without the LoS link respectively. Considering a multiple-relay scenario, the work in [11] investigated the OP performance of decode-and-forward HSTRNs with the best relay selection strategy. Moreover, the authors in [12] studied the bit error rate performance of HSTRNs with CCI at the relay and destination nodes. Despite the benefit of the HSTRNs, more resource consumption, such as the extra power consumption at the relay node, in the HSTRNs cannot meet the increasing demands for reducing power consumption and

X. Yan and H. Xiao (corresponding author) are with the Key Laboratory of Cognitive Radio and Information Processing (Guilin University of Electronic Technology), Ministry of Education, Guilin 541004, China, X. Yan is also with the Engineering Training Center, Qinzhou University, Qinzhou 535011, China (e-mail: yxj9609@163.com, xhl_xiaohailin@163.com).

C.-X. Wang is with the Institute of Sensors, Signals, and Systems, School of Engineering and Physical Sciences, Heriot-Watt University, Edinburgh EH14 4AS, U.K. (e-mail: cheng-xiang.wang@hw.ac.uk).

K. An is with the National University of Defense Technology, Nanjing 210007, China (e-mail: ankang@nuaa.edu.cn).

A. T. Chronopoulos is with the Department of Computer Science, University of Texas San Antonio, TX 78249 and Visiting Faculty at the Department of Computer Science, University of Patras, Greece (e-mail: antony.tc@gmail.com).

G. Zheng is with the Wolfson School of Mechanical, Electrical, and Manufacturing Engineering, Loughborough University, Loughborough LE11 3TU, U.K. (e-mail: g.zheng@lboro.ac.uk).

The authors gratefully acknowledge the support from the National Natural Science Foundation of China under Grants 61471392, 61472094, and 61261018, the EPSRC TOUCAN project (No. EP/L020009/1), the EU FP7 QUICK project (No. PIRSES-GA-2013-612652), the EU H2020 RISE TESTBED project (No. 734325), the UK EPSRC under grant EP/N007840/1, the Innovation Project of Guangxi Graduate Education, and the Innovation Project of GUET Graduate Education (No. 2016YJCXB05).

devising energy-efficient network components.

The aforementioned papers have considered different architectures to improve the spectrum efficiency and reliability of satellite systems based on the existing satellite platform. However, the key limitation is that almost all of those works adopted a orthogonal multiple access (OMA) scheme. Since only one user can be served at any time/frequency slot, OMA scheme can effectively avoid interference between users, but it also restricts the resource utilization efficiency. Furthermore, OMA scheme prefers to serve user with good link condition and the fairness of user with deteriorated link quality would be sacrificed. While in future satellite networks, high quality of service (QoS) to a large number of users is required. Under this condition, other multiple access schemes should be taken into account to improve the spectrum efficiency and lower the resource consumption in future satellite communications.

Having the ability to provide high spectrum efficiency and energy efficiency (EE) [13], non-orthogonal multiple access (NOMA) scheme has recently received significant attentions. With the NOMA scheme, multiple signals are superposed in power domain and transmitted simultaneously over the same frequency/time channel, successive interference cancellation (SIC) is applied at the receiver side to remove the interference caused by superposition coding [14]–[17]. In this regard, more NOMA users are possible to gain access than OMA. Many works have investigated the performance of NOMA scheme from the perspective of power allocation or user selection strategy with different objectives. Taking the minimization of transmission power as target, the authors in [18] proposed a jointly searching for subcarrier and power allocations scheme. A general power allocation strategy was proposed in [19] by assuming that the NOMA scheme always outperforms the time division multiple access (TDMA) scheme. In addition, the authors in [20] and [21] conducted performance investigation of NOMA with different user scheduling strategies in visible light communication and integrated satellite terrestrial networks scenarios, respectively. Recently, the authors in [22] and [23] integrated the NOMA scheme into hybrid satellite terrestrial relay networks to further improve the OP for users whose direct links were unavailable. However, works [22] and [23] mainly conducted performance evaluation based on a fixed power allocation factor, without considering the optimal power allocation strategy in a scenario where users can link with the satellite directly.

To fill the above research gaps as well as meet the requirements of both performance and energy efficiency (EE) in future satellite communications, in this paper, we propose a NOMA-based transmission scheme for the LMS systems, in which a two-user downlink case of NOMA group for satellite communications is considered. Particularly, our main contributions can be summarized as follows:

- In light of the state-of-art propagation model, we employ a general framework for NOMA-based LMS systems by considering channel statistical prosperity, propagation loss and geometric antenna pattern. Based on which, the power allocation coefficients in terms of maximizing the sum rate of LMS system while meeting the predefined target rate of each NOMA user are then obtained.

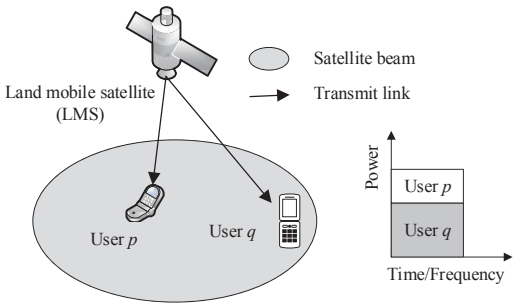

Fig. 1. System model of NOMA-based downlink LMS network.

- Theoretical expressions for the ergodic capacity and EE performances of the considered LMS system are derived, which provides an effective approach to evaluate the effect of various parameters, such as the fading configurations of the satellite links, on the performance of the considered system.
- To further analyze the QoS and reliability performance, analytical expressions for the OP and ASER of the each NOMA user are further derived, which provide further guidance on user selection strategy when forming a NOMA group. Meanwhile, the asymptotic yet simple OP expressions at the high signal-to-noise ratio (SNR) regime are also derived for NOMA users to characterize two important performance merits, i.e., the achievable diversity order and coding gain.

The rest of this paper is outlined as follows. Section II presents the system model and describes the related channel models. In section III, we derive the theoretical expressions for the ergodic capacity, EE, OP, asymptotic OP, and ASER. In Section IV, simulation results and discussions are provided and conclusions are drawn in Section V.

II. SYSTEM MODEL

As shown in Fig.1, a LMS simultaneously communicates with two terrestrial users, User p and User q, with the help of the NOMA scheme. It is assumed that User p and User q are located in the same spot beam[1] but with different positions. All nodes in the proposed model are also assumed to equip with a single antenna for simplicity. It is worth noting that only two-user cluster is considered in this paper because this form of NOMA has been included in the Third Generation Partnership Project (3GPP)–Long Term Evolution (LTE) Advanced [17]. Moreover, the authors in [24] investigated the performance of MIMO-NOMA in terms of the sum channel capacity and ergodic sum capacity. One of the most important conclusions that can be drawn from [24] is that a lower sum rate can be obtained when more than two users are admitted into a cluster.

A. Channel Model

Since mobile satellite service systems which operate at frequency bands well below 10 GHz in propagation environments

[1]Although multibeam technology has been widely adopted in satellite networks, here we consider one of the spot beam coverage area for simplicity.

suffer from different levels of obstruction [25]. The satellite channel model including beam gain, fading model, and free space loss (FSL) is described in the following.

1) Beam gain: Given the position of User j ($j = p, q$), define φ_j to denote the angle between User j and the beam center with respect to the satellite, the beam gain $G_j(\varphi_j)$ can be calculated as [26]

$$G_j(\varphi_j) = G_j \left(\frac{J_1(u_j)}{2u_j} + 36\frac{J_3(u_j)}{u_j^3} \right)^2 \tag{1}$$

where G_j denotes the antenna gain at User j, $J(\cdot)$ is the Bessel function and $u_j = 2.07123\frac{\sin\varphi_j}{\sin\varphi_{j3\mathrm{dB}}}$ with $\varphi_{j3\mathrm{dB}}$ being the 3-dB angle.

2) Fading model: Similar to [5] and [6], we assume the links between satellite and terrestrial destinations are undergoing independent and identically distributed (i.i.d.) shadowed-Rician fading distribution. The shadowed-Rician fading channel is widely employed in existing literatures because it not only facilitates the mathematic computation but also sufficiently describes the characteristic of satellite terrestrial link. According to [27], the probability density function (PDF) of the fading gain, $|h_j|^2$, is given as

$$f_{|h_j|^2}(x) = \alpha_j e^{-\beta_j x} {}_1F_1(m_j; 1; \delta_j x) \tag{2}$$

where $\alpha_j = 0.5(2b_jm_j/(2b_jm_j + \Omega_j))^{m_j}/b_j$, $\beta_j = 0.5/b_j$, $\delta_j = 0.5\Omega_j/b_j/(2b_jm_j + \Omega_j)$, $2b_j$ and Ω_j are the average power of the multipath component and LoS component, respectively, m_j ($m_j > 0$) denotes the Nakagami-m parameter, and ${}_1F_1(a; b; c)$ represents the confluent hypergeometric function [28, (9.100)].

3) FSL: The FSL can be calculated as [26]

$$L_j = \left(\frac{c}{4\pi f_c d_j} \right)^2 \tag{3}$$

where c is the light speed, f_c is the frequency, d_j is link distance from the satellite to User j.

Note that users within a beam area may experience similar FSL towards the satellite [29], but significant differences in users' channel gains still can be observed due to different propagations, such as different positions and masking effects. To ensure that User p has a better channel quality than that of User q, we consider $L_qG_q(\varphi_q)|h_q|^2 < L_pG_p(\varphi_p)|h_p|^2$ in our next Sections if without other description.

B. Signal Model

By applying the NOMA scheme, the LMS can broadcast a superposed signal x ($x = \sqrt{\alpha P_\mathrm{s}}x_p + \sqrt{(1-\alpha)P_\mathrm{s}}x_q$) to satellite users, the received signal at User j ($j = p, q$) is

$$y_j = \sqrt{L_jG_sG_j(\varphi_j)}h_jx + n_j \tag{4}$$

where G_s is the antenna gain at the satellite, α ($0 \le \alpha \le 1$) denotes a fraction of the transmit power P_s allocated to User p, x_j ($\mathrm{E}\left[|x_j|^2\right] = 1$) is the transmission signal for User j, and n_j denotes the additive white Gaussian noise (AWGN) with $\mathrm{E}\left[|n_j|^2\right]$=$N_0$. According to the principle of the NOMA scheme, the user with the worse channel quality decodes its own information directly. Thus, the instantaneous end-to-end SINR of User q can be expressed as

$$\gamma_q = \frac{(1-\alpha)P_\mathrm{s}Q_q|h_q|^2}{\alpha Q_qP_\mathrm{s}|h_q|^2 + N_0} \tag{5}$$

where Q_q=$L_qG_sG_q(\varphi_q)$. Based on the criterion of SIC, user with good channel gain, User p, first decodes the information from User q. In this paper, the decoding SINR is

$$\gamma_{p\to q} = \frac{(1-\alpha)Q_pP_\mathrm{s}|h_p|^2}{\alpha Q_pP_\mathrm{s}|h_p|^2 + N_0} \tag{6}$$

where Q_p=$L_pG_sG_p(\varphi_p)$. Compare (5) with (6), we can find that $\gamma_{p\to q}$ is more than γ_q because of the assumption $Q_p > Q_q$, implying that the information of User *q* could be correctly decoded at User *p*. After subtracting the decoded information, User p decodes its own information and the SINR of User p can be written as

$$\gamma_p = \frac{\alpha P_\mathrm{s}Q_p|h_p|^2}{N_0}. \tag{7}$$

Then, the sum rate of the considered system can be written as

$$\begin{aligned} R_\mathrm{sum} &= R_p^\mathrm{NOMA} + R_q^\mathrm{NOMA} \\ &= \log_2\left(1 + \frac{\alpha P_\mathrm{s}Q_p|h_p|^2}{N_0}\right) + \log_2\left(1 + \frac{(1-\alpha)P_\mathrm{s}Q_q|h_q|^2}{\alpha P_\mathrm{s}Q_q|h_q|^2 + N_0}\right). \end{aligned} \tag{8}$$

In addition, to assure that the transmission rate with the NOMA scheme always outperforms that with the TDMA scheme [19], the range of α can be further constrained as

$$\alpha_1 \le \alpha \le \alpha_2 \tag{9}$$

where $\alpha_1 = \frac{1}{\sqrt{1+\bar{\gamma}Q_p|h_p|^2}+1}$, $\alpha_2 = \frac{1}{\sqrt{1+\bar{\gamma}Q_q|h_q|^2}+1}$, and $\bar{\gamma} = P_\mathrm{s}/N_0$ is the transmission average SNR. Specifically, we can easily derive that $\alpha_1 < \alpha_2 < 0.5$ due to $Q_p > Q_q \ge 0$. The derivation of α_1 and α_2 can be found in Appendix A.

Since the first derivative of R_sum with respect to α is strictly positive, which implies that the sum rate is increasing with α. Therefore, taking the constraint of (9) into consideration, the maximization of sum rate is obtained when $\alpha = \alpha_2$. Under this condition, the SINR at Users p and q can be derived as

$$\gamma_p = \frac{\bar{\gamma}Q_p|h_p|^2}{\sqrt{1+\bar{\gamma}Q_q|h_q|^2}+1} \tag{10}$$

and

$$\gamma_q = \sqrt{1+\bar{\gamma}Q_q|h_q|^2} - 1. \tag{11}$$

It is worth noting that the transmission rate of User *p* or User *q* with NOMA scheme is equal to that with TDMA scheme, when $\alpha = \alpha_1$ or $\alpha = \alpha_2$. If the power allocation coefficient is set as $\alpha = \alpha_2$, then we can find that the sum rate gap between NOMA and TDMA stems from the transmission rate of User *p*, and the gap $R_\mathrm{gap} = \log_2\left(1 + (\alpha_2 - \alpha_1)\bar{\gamma}Q_p|h_p|^2\right)$.

III. PERFORMANCE ANALYSIS

In this section, with the help of Meijer-G functions, we present a comprehensive framework to analyze the performance of the considered network. Specifically, we derive analytical expressions for five performance metrics, i.e., ergodic capacity, EE, OP, asymptotic OP, and ASER.

A. Ergodic capacity

The ergodic capacity is defined as the expected value of the instantaneous end-to-end mutual information [8], which can be expressed as

$$C_{\rm erg} = \mathrm{E}\left[\log_2\left(1+\gamma_p\right)\right] + \mathrm{E}\left[\log_2\left(1+\gamma_q\right)\right]. \quad (12)$$

By substituting (10) and (11) into (12), along with some manipulations, $C_{\rm erg}$ can be rewritten as

$$C_{\rm erg} = \underbrace{\mathrm{E}\left[\log_2\left(1+\bar{\gamma}Q_p|h_p|^2+\sqrt{1+\bar{\gamma}Q_q|h_q|^2}\right)\right]}_{I_1} - \underbrace{\mathrm{E}\left[\log_2\left(1+1\Big/\sqrt{1+\bar{\gamma}Q_q|h_q|^2}\right)\right]}_{I_2}. \quad (13)$$

To evaluate the ergodic capacity of the proposed network, we compute I_1 and I_2 in the following subsections.

1) Result for I_1:

Since the closed-form expression for I_1 is mathematically intractable, we seek to consider the approximation expression as well as lower and upper bounds for I_1 in this subsection.

Analytical approximation: With the help of [30], I_1 can be well approximated as

$$I_1 \approx \log_2(e)\left[\ln(1+\mathrm{E}[I_3]) - \frac{\mathrm{E}\left[I_3^2\right]-\mathrm{E}^2[I_3]}{2\left(1+\mathrm{E}[I_3]\right)^2}\right] \quad (14)$$

with

$$I_3 = \bar{\gamma}Q_p|h_p|^2+\sqrt{1+\bar{\gamma}Q_q|h_q|^2}. \quad (15)$$

Since $|h_p|^2$ and $|h_q|^2$ are mutually independent, we have

$$\mathrm{E}[I_3] = \mathrm{E}\left[\bar{\gamma}Q_p|h_p|^2\right] + \mathrm{E}\left[\sqrt{1+\bar{\gamma}Q_q|h_q|^2}\right], \quad (16)$$

$$\mathrm{E}\left[I_3^2\right] = \mathrm{E}\left[\bar{\gamma}^2Q_p^2|h_p|^4\right] + \mathrm{E}\left[1+\bar{\gamma}Q_q|h_q|^2\right] + 2\mathrm{E}\left[\bar{\gamma}Q_p|h_p|^2\right]\mathrm{E}\left[\sqrt{1+\bar{\gamma}Q_q|h_q|^2}\right]. \quad (17)$$

Now, we start with the n^{th}-order moment of $\bar{\gamma}Q_p|h_p|^2$, which can be derived as

$$\mathrm{E}\left[\left(\bar{\gamma}Q_px\right)^n\right] = \bar{\gamma}^nQ_p^n\int_0^\infty x^n f_{|h_p|^2}(x)\,dx. \quad (18)$$

To compute (18), we exploit ${}_1F_1(a;b;c)$ [28, (8.455.1)] in terms of Meijer-G functions as

$${}_1F_1\left(m_p;1;\delta_px\right) = \frac{1}{\Gamma(m_p)}G_{1,2}^{1,1}\left[-\delta_px\,\middle|\,\begin{matrix}1-m_p\\0,0\end{matrix}\right] \quad (19)$$

where $G_{1,2}^{1,1}[\cdot|\cdot]$ [28, (9.301)] is the Meijer-G function and $\Gamma(\cdot)$ [28, (8.310.1)] is the Gamma function. Inserting (2) and (19) into (18) along with [28, (7.813.1)], we get

$$\mathrm{E}\left[\left(\bar{\gamma}Q_px\right)^n\right] = \frac{\alpha_p\bar{\gamma}^nQ_p^n}{\Gamma(m_p)\,\beta_p^{n+1}}G_{2,2}^{1,2}\left[\frac{-\delta_p}{\beta_p}\,\middle|\,\begin{matrix}-n,1-m_p\\0,0\end{matrix}\right]. \quad (20)$$

Since the PDFs of $f_{|h_p|^2}(x)$ and $f_{|h_q|^2}(y)$ have the same form, following similar steps as that in the derivation of (18), we get

$$\mathrm{E}\left[1+\bar{\gamma}Q_qy\right] = \int_0^\infty\left(1+\bar{\gamma}Q_qy\right)f_{|h_q|^2}(y)dy = 1+\frac{\alpha_q\bar{\gamma}Q_q}{\Gamma(m_q)\,\beta_q^2}G_{2,2}^{1,2}\left[\frac{-\delta_q}{\beta_q}\,\middle|\,\begin{matrix}-1,1-m_q\\0,0\end{matrix}\right]. \quad (21)$$

To solve $\mathrm{E}\left[\sqrt{1+\bar{\gamma}Q_qy}\right]$, we first express $\sqrt{1+\bar{\gamma}Q_qy}$ in terms of Meijer-G functions based on [31, (10)] as

$$\left(1+\bar{\gamma}Q_qy\right)^{0.5} = \frac{1}{\Gamma(-0.5)}G_{1,1}^{1,1}\left[\bar{\gamma}Q_qy\,\middle|\,\begin{matrix}1.5\\0\end{matrix}\right]. \quad (22)$$

Then, with the aid of [32, (2.6.2)], we get

$$\mathrm{E}\left[\sqrt{1+\bar{\gamma}Q_qy}\right] = \frac{\alpha_q}{\Gamma(-0.5)\,\Gamma(m_q)\,\beta_q} \times G_{1,[1:1],0,[1:2]}^{1,1,1,1,1}\left[\begin{matrix}\frac{\bar{\gamma}Q_q}{\beta_q}\\ \\ \frac{-\delta_q}{\beta_q}\end{matrix}\,\middle|\,\begin{matrix}1\\1.5;1-m_q\\--\\0;0,0\end{matrix}\right] \quad (23)$$

where $G_{1,[1:1],0,[1:2]}^{1,1,1,1,1}[\dot{\cdot}|\cdot]$ [33] is the generalized Meijer-G functions with two variables, which can be computed with the method proposed in [34]. By substituting (20), (21), and (23) into (14), the desired result for the approximate expression of I_1 can be evaluated as (24) at the top of next page.

Lower bound: Using Jesens inequality [35], we can express the lower bound of I_1 as

$$I_1 \geq \log_2\left(1+e^{\mathrm{E}\left[\ln\left(\sqrt{1+\bar{\gamma}Q_qy}\right)\right]}+e^{\mathrm{E}\left[\ln\left(\bar{\gamma}Q_px\right)\right]}\right) \quad (25)$$

where $\ln(1+\bar{\gamma}Q_qy)$ [31, (11)] can be written as

$$\ln\left(1+\bar{\gamma}Q_qy\right) = G_{2,2}^{1,2}\left[\bar{\gamma}Q_qy\,\middle|\,\begin{matrix}1,1\\1,0\end{matrix}\right]. \quad (26)$$

Combining (2), (19), and (26) in conjunction with [32, (2.6.2)], we have

$$\mathrm{E}\left[\ln\left(\sqrt{1+\bar{\gamma}Q_qy}\right)\right] = \frac{0.5\alpha_q}{\Gamma(m_q)\,\beta_q} \times G_{1,[2:1],0,[2:2]}^{1,2,1,1,1}\left[\begin{matrix}\frac{\bar{\gamma}Q_q}{\beta_q}\\ \\ \frac{-\delta_q}{\beta_q}\end{matrix}\,\middle|\,\begin{matrix}1\\1,1;1-m_q\\--\\1,0;0,0\end{matrix}\right]. \quad (27)$$

Further, using (2) along with [28, (9.14.1), (4.352.1)], $\mathrm{E}\left[\ln\left(\bar{\gamma}Q_px\right)\right]$ can be derived as

$$\mathrm{E}\left[\ln\left(\bar{\gamma}Q_px\right)\right] = \ln\bar{\gamma}Q_p + \alpha_p\sum_{k=0}^{\infty}\frac{(m_p)_k\delta_p^k}{\beta_p^{k+1}}\left[\psi(k+1)-\ln(\beta_p)\right] \quad (28)$$

where $(x)_k = \Gamma(x+k)/\Gamma(x)$ [28] is the Pochhammer symbol, $\psi(\cdot)$ [28, (8.360)] is the Euler psi function. Substituting (27)

$$
\begin{aligned}
I_1 \approx \log_2(e)\ln\Bigg\{ & 1+\tfrac{\alpha_p\bar{\gamma}Q_p}{\Gamma(m_p)\beta_p^2}G_{2,2}^{1,2}\left[\tfrac{-\delta_p}{\beta_p}\middle|\begin{matrix}-1,1-m_p\\0,0\end{matrix}\right]+\tfrac{\alpha_q}{\Gamma(-0.5)\Gamma(m_q)\beta_q}G_{1,[1:1],0,[1:2]}^{1,1,1,1,1}\left[\begin{matrix}\frac{\bar{\gamma}Q_q}{\beta_q}\\ \\ \frac{-\delta_q}{\beta_q}\end{matrix}\middle|\begin{matrix}1\\1.5;1-m_q\\--\\0;0,0\end{matrix}\right] \\
& -\Bigg\{1+\tfrac{\alpha_p\bar{\gamma}^2Q_p^2}{\Gamma(m_p)\beta_p^3}G_{2,2}^{1,2}\left[\tfrac{-\delta_p}{\beta_p}\middle|\begin{matrix}-2,1-m_p\\0,0\end{matrix}\right]+\tfrac{\alpha_q\bar{\gamma}Q_q}{\Gamma(m_q)\beta_q^2}G_{2,2}^{1,2}\left[\tfrac{-\delta_q}{\beta_q}\middle|\begin{matrix}-1,1-m_q\\0,0\end{matrix}\right] \\
& +\tfrac{2\alpha_p\bar{\gamma}\alpha_qQ_p}{\Gamma(m_p)\beta_p^2\Gamma(-0.5)\Gamma(m_q)\beta_q}G_{2,2}^{1,2}\left[\tfrac{-\delta_p}{\beta_p}\middle|\begin{matrix}-1,1-m_p\\0,0\end{matrix}\right]G_{1,[1:1],0,[1:2]}^{1,1,1,1,1}\left[\begin{matrix}\frac{\bar{\gamma}Q_q}{\beta_q}\\ \\ \frac{-\delta_q}{\beta_q}\end{matrix}\middle|\begin{matrix}1\\1.5;1-m_q\\--\\0;0,0\end{matrix}\right] \\
& -\left[\tfrac{\alpha_p\bar{\gamma}Q_p}{\Gamma(m_p)\beta_p^2}G_{2,2}^{1,2}\left[\tfrac{-\delta_p}{\beta_p}\middle|\begin{matrix}-1,1-m_p\\0,0\end{matrix}\right]+\tfrac{\alpha_q}{\Gamma(-0.5)\Gamma(m_q)\beta_q}G_{1,[1:1],0,[1:2]}^{1,1,1,1,1}\left[\begin{matrix}\frac{\bar{\gamma}Q_q}{\beta_q}\\ \\ \frac{-\delta_q}{\beta_q}\end{matrix}\middle|\begin{matrix}1\\1.5;1-m_q\\--\\0;0,0\end{matrix}\right]\right]^2\Bigg\} \\
& \div\left\{2\left[1+\tfrac{\alpha_p\bar{\gamma}Q_p}{\Gamma(m_p)\beta_p^2}G_{2,2}^{1,2}\left[\tfrac{-\delta_p}{\beta_p}\middle|\begin{matrix}-1,1-m_p\\0,0\end{matrix}\right]+\tfrac{\alpha_q}{\Gamma(-0.5)\Gamma(m_q)\beta_q}G_{1,[1:1],0,[1:2]}^{1,1,1,1,1}\left[\begin{matrix}\frac{\bar{\gamma}Q_q}{\beta_q}\\ \\ \frac{-\delta_q}{\beta_q}\end{matrix}\middle|\begin{matrix}1\\1.5;1-m_q\\--\\0;0,0\end{matrix}\right]\right]^2\right\}\Bigg\}.
\end{aligned}
\tag{24}
$$

$$
I_1 \geq B\log_2\left\{1+Exp\left[\frac{0.5\alpha_q}{\Gamma(m_q)\beta_q}G_{1,[2:1],0,[2:2]}^{1,2,1,1,1}\left[\begin{matrix}\frac{\bar{\gamma}Q_q}{\beta_q}\\ \\ \frac{-\delta_q}{\beta_q}\end{matrix}\middle|\begin{matrix}1\\1,1;1-m_q\\--\\1,0;0,0\end{matrix}\right]\right]+Exp\left[\ln\bar{\gamma}Q_p+\alpha_p\sum_{k=0}^{\infty}\frac{(m_p)_k\delta_p^k}{\beta_p^{k+1}}\left[\psi(\cdot)-\ln(\beta_p)\right]\right]\right\}. \tag{29}
$$

$$
I_1 \leq B\log_2\left\{1+\frac{\alpha_p\bar{\gamma}Q_p}{\Gamma(m_p)\beta_p^2}G_{2,2}^{1,2}\left[\frac{-\delta_p}{\beta_p}\middle|\begin{matrix}-1,1-m_p\\0,0\end{matrix}\right]+\frac{\alpha_q}{\Gamma(-0.5)\Gamma(m_q)\beta_q}G_{1,[1:1],0,[1:2]}^{1,1,1,1,1}\left[\begin{matrix}\frac{\bar{\gamma}Q_q}{\beta_q}\\ \\ \frac{-\delta_q}{\beta_q}\end{matrix}\middle|\begin{matrix}1\\1.5;1-m_q\\--\\0;0,0\end{matrix}\right]\right\}. \tag{31}
$$

and (28) together into (25), the lower bound of I_1 can be straightforwardly obtained as shown in (29).

Upper bound: According to the results reported in [35], I_1 can be upper bounded by

$$
I_1 \leq \log_2\left(1+\mathrm{E}\left[\bar{\gamma}Q_px\right]+\mathrm{E}\left[\sqrt{1+\bar{\gamma}Q_qy}\right]\right). \tag{30}
$$

Since we have derived $\mathrm{E}\left[\sqrt{1+\bar{\gamma}Q_qy}\right]$ by (23) and $\mathrm{E}\left[\bar{\gamma}Q_px\right]$ by (20) with $n=1$, the upper bound can be derived as (31).

2) Result for I_2:

To obtain I_2, we express $\mathrm{E}\left[\ln\left(1+(1+\bar{\gamma}y)^{-0.5}\right)\right]$ into series representations with [28, (1.511)], i.e.,

$$
\mathrm{E}\Big[\ln\left(1+(1+\bar{\gamma}y)^{-0.5}\right)\Big]=\sum_{n=1}^{\infty}(-1)^{n+1}\mathrm{E}\left[\frac{(1+\bar{\gamma}y)^{-\frac{n}{2}}}{n}\right]. \tag{32}
$$

Then, combining (2), (19), and (32) along with the help of [31, (10)] and [32, (2.6.2)], we further obtain

$$
\begin{aligned}
I_2=\sum_{n=1}^{\infty}\frac{\alpha_q(-1)^{n+1}}{n\Gamma(0.5n)\Gamma(m_q)\beta_q\ln 2} & \\
\times G_{1,[1:1],0,[2:1]}^{1,1,1,1,1}\left[\begin{matrix}\frac{-\delta_q}{\beta_q}\\ \\ \frac{\bar{\gamma}}{\beta_q}\end{matrix}\middle|\begin{matrix}1\\1-m_q;1-0.5n\\--\\0,0;0\end{matrix}\right]. &
\end{aligned}
\tag{33}
$$

Finally, based on the above derived results, an approximation as well as the upper and lower bounds of (13) have all be obtained.

B. Energy efficiency

In the LMS networks which powered by solar panels or batteries, more reliable transmission is commonly achieved at the expense of more transmission power consumed. However, in practice, the recharge/discharge cycles of batteries are limited even if the power supply is sufficient. In this case, taking EE as a performance criteria is more meaningful than considering transmission rate only. For the NOMA–based LMS networks, the EE [36] can be mathematically derived as

$$
\eta_{\mathrm{EE}}=\frac{R_{\mathrm{sys}}}{\xi P_{\mathrm{s}}+P_{\mathrm{int}}} \tag{34}
$$

where R_{sys} is the system sum rate, $\xi>1$ is related to the efficiency of power amplifier, P_{int} is the fixed power consumption including circuit power and other overheads. In this paper, we set $R_{\mathrm{sys}}=C_{\mathrm{erg}}$. Then, we can get $\eta_{\mathrm{EE}}=\frac{C_{\mathrm{erg}}}{\xi P_{\mathrm{s}}+P_{\mathrm{int}}}$.

C. Outage probability

The OP is defined as the probability that γ_j $(j=p,q)$ falls below a predefined threshold γ_{th} [37], which can be

mathematically expressed as

$$P_{\text{out}}\left(\gamma_{\text{th}}\right)=P\left\{\gamma_j\leq\gamma_{\text{th}}\right\}=F_{\gamma_j}\left(\gamma_{\text{th}}\right) \tag{35}$$

where $F_{\gamma_j}(\cdot)$ is the cumulative distribution function (CDF) of γ_j. To evaluate the OP performances of Users p and q, we first derive the CDF of $|h_j|^2$ with the aid of [28, (9.14.1), (3.381.1)] as

$$F_{|h_j|^2}(u)=\alpha_j\sum_{k=0}^{\infty}\frac{(m_j)_k\delta_j^k}{(k!)^2\beta_j^{k+1}}\gamma\left(k+1,\beta_j u\right) \tag{36}$$

where $\gamma(a,x)$ [28, (8.354.1)] is the incomplete Gamma function. Based on (36), we will derive the exact OP expressions for NOMA users in the following:

1) The OP of User p:

From (10), the CDF of γ_p can be derived as

$$\begin{aligned}F_{\gamma_p}\left(\gamma_{\text{th}}\right)&=P\left\{|h_p|^2\leq\frac{\gamma_{\text{th}}\left(\sqrt{1+\bar{\gamma}Q_q|h_q|^2}+1\right)}{\bar{\gamma}Q_p}\right\}\\&=\int_0^{\infty}F_x\left(\frac{\gamma_{\text{th}}\left(\sqrt{1+\bar{\gamma}Q_q y}+1\right)}{\bar{\gamma}Q_p}\right)f_{|h_q|^2}(y)\,dy.\end{aligned} \tag{37}$$

By substituting (2) and (36) into (37), we can get

$$\begin{aligned}F_{\gamma_p}\left(\gamma_{\text{th}}\right)&=\alpha_p\sum_{k=0}^{\infty}\frac{(m_p)_k\delta_p^k}{(k!)^2\beta_p^{k+1}}\\&\times\int_0^{\infty}\gamma\left(k+1,\frac{\beta_p\gamma_{\text{th}}\left(\sqrt{1+\bar{\gamma}Q_q y}+1\right)}{\bar{\gamma}Q_p}\right)f_{|h_q|^2}(y)dy.\end{aligned} \tag{38}$$

To solve the integral in (38), $\gamma\left(k+1,\frac{\beta_p\gamma_{th}\left(\sqrt{1+\bar{\gamma}Q_q y}+1\right)}{\bar{\gamma}Q_p}\right)$ can be expressed into series according to [28, (8.354.1)] as

$$\begin{aligned}&\gamma\left(k+1,\frac{\beta_p\gamma_{th}\left(\sqrt{1+\bar{\gamma}Q_q y}+1\right)}{\bar{\gamma}Q_p}\right)\\&=\sum_{n=0}^{\infty}\frac{(-1)^n}{n!w}\left(\frac{\beta_p\gamma_{\text{th}}}{\bar{\gamma}Q_p}\right)^w\sum_{t=0}^{w}\binom{w}{t}(1+\bar{\gamma}Q_q y)^{\frac{t}{2}}\end{aligned} \tag{39}$$

where $w=k+n+1$. To this end, by combing (39) and (2) along with the help of [31, (10)] and [32, (2.6.2)], $F_{\gamma_p}(\gamma_{\text{th}})$ can be calculated as

$$\begin{aligned}&F_{\gamma_p}\left(\gamma_{\text{th}}\right)\\&=\alpha_p\sum_{k=0}^{\infty}\sum_{n=0}^{\infty}\sum_{t=0}^{w}\binom{w}{t}\frac{(m_p)_k\delta_p^k(-1)^n\alpha_q}{(k!)^2\beta_p^{k+1}n!w\Gamma(-0.5t)\Gamma(m_q)\beta_q}\\&\times\left(\frac{\beta_p\gamma_{\text{th}}}{\bar{\gamma}Q_p}\right)^w G_{1,[1:1],0,[1:2]}^{1,1,1,1,1}\left[\begin{array}{c|c}\frac{\bar{\gamma}Q_q}{\beta_q} & 1\\ & 1+0.5t;1-m_q\\ \frac{-\delta_q}{\beta_q} & --\\ & 0,0;0\end{array}\right].\end{aligned} \tag{40}$$

2) The OP of User q:

Since the PDFs of x and y have the same form, from (11), we can derive the CDF of User q as

$$F_{\gamma_q}(\gamma_{\text{th}})=P\left\{|h_q|^2\leq\frac{\gamma_{\text{th}}\left(\gamma_{\text{th}}+2\right)}{\bar{\gamma}Q_q}\right\}=F_y\left(\frac{\gamma_{\text{th}}\left(\gamma_{\text{th}}+2\right)}{\bar{\gamma}Q_q}\right). \tag{41}$$

After substituting (36) into (41), we have

$$F_{\gamma_q}(\gamma_{\text{th}})=\alpha_q\sum_{k=0}^{\infty}\frac{(m_q)_k\delta_q^k}{(k!)^2\beta_q^{k+1}}\gamma\left(k+1,\beta_q\frac{\gamma_{\text{th}}\left(\gamma_{\text{th}}+2\right)}{\bar{\gamma}Q_q}\right). \tag{42}$$

D. Asymptotic OP analysis at the high SNR

Based on the studies reported in [38], the diversity order G_{d} and coding gain G_{c} of the considered system can be easily obtained by evaluating the asymptotic OP performance at the high SNR regime, as

$$F_{\gamma_p}^{\infty}\left(\gamma_{\text{th}}\right)\approx\left(G_{\text{c}}\bar{\gamma}\right)^{-G_{\text{d}}}. \tag{43}$$

To evaluate the asymptotic OP performance, for simplicity, we expand $\gamma(a,x)$ into series and obtain

$$\gamma(a,x)=\sum_{n=0}^{\infty}\frac{(-1)^n x^{a+n}}{n!\left(a+n\right)}\approx\frac{x^a}{a}\,|_{x\to 0}\,. \tag{44}$$

Hence, by substituting (44) into (36), the CDF of $|h_j|^2$ can be approximated as

$$F_{|h_j|^2}^{\infty}(u)\approx\alpha_j u\,|_{u\to 0}\,. \tag{45}$$

Based on (45), we seek to derive the asymptotic OP expressions for NOMA users as follows:

1) Asymptotic OP of User p:

Substituting (45) into (37), we have

$$F_{\gamma_p}^{\infty}\left(\gamma_{\text{th}}\right)\approx\alpha_p\frac{\gamma_{\text{th}}}{\bar{\gamma}Q_p}\int_0^{\infty}\left(\sqrt{1+\bar{\gamma}Q_q y}+1\right)f_{|h_q|^2}(y)\,dy. \tag{46}$$

With the help of [28, (9.14.1)] and [31, (10)], we get

$$\begin{aligned}F_{\gamma_p}^{\infty}\left(\gamma_{\text{th}}\right)\approx&\alpha_p\frac{\gamma_{\text{th}}}{\bar{\gamma}Q_p}+\alpha_p\frac{\gamma_{\text{th}}}{\bar{\gamma}Q_p}\sum_{k=0}^{\infty}\frac{\alpha_q(m_q)_k\delta_q^k}{\Gamma(-0.5)(k!)^2\beta_q^{k+1}}\\&\times G_{2,1}^{1,2}\left[\frac{\bar{\gamma}Q_q}{\beta_q}\,\middle|\,\begin{matrix}-k,1.5\\0\end{matrix}\right].\end{aligned} \tag{47}$$

To compute (47), we first expand $G_{2,1}^{1,2}\left[\frac{\bar{\gamma}Q_q}{\beta_q}\,\middle|\,\begin{matrix}-k,1.5\\0\end{matrix}\right]$ into series according to [28, (9.304), (9.14.1)], as

$$\begin{aligned}&G_{2,1}^{1,2}\left[\frac{\bar{\gamma}Q_q}{\beta_q}\,\middle|\,\begin{matrix}-k,1.5\\0\end{matrix}\right]|_{\bar{\gamma}\to\infty}\\&=\Gamma(k+1)\Gamma(-k-1.5)\left(\frac{\beta_q}{\bar{\gamma}Q_q}\right)^{k+1}\\&+\Gamma(-0.5)\Gamma(k+1.5)\left(\frac{\bar{\gamma}Q_q}{\beta_q}\right)^{0.5}.\end{aligned} \tag{48}$$

Then, by putting (48) into (47), the asymptotic OP of User p is given by

$$\begin{aligned}F_{\gamma_p}^{\infty}\left(\gamma_{\text{th}}\right)\approx&\alpha_p\frac{\gamma_{\text{th}}}{\bar{\gamma}Q_p}+\frac{2\alpha_q\alpha_p\gamma_{\text{th}}}{3\bar{\gamma}^2Q_pQ_q}\\&+\alpha_p\alpha_q\gamma_{\text{th}}\underbrace{\sum_{k=0}^{\infty}\frac{(m_q)_k\delta_q^k\Gamma(k+1.5)Q_q^{0.5}}{(k!)^2\beta_q^{k+1.5}Q_p}}_{I_5}\bar{\gamma}^{-0.5}.\end{aligned} \tag{49}$$

Despite the infinite sum expressions involved in I_5, it can be easily evaluated numerically, i.e., $Q_p=Q_q=1$, $I_5=0.04$ if User q undergoes heavy shadowing (HS) link, and $I_5=4.33$ if User q experiences average shadowing (AS) link. Thus, at the high SNR regime, the third term of (49) has a predominant effect on the asymptotic OP performance. So, we can get $F_{\gamma_p}^{\infty}(\gamma_{\text{th}})\approx\gamma_{\text{th}}\alpha_p\alpha_q I_5\bar{\gamma}^{-0.5}$, and further obtain the diversity order and coding gain for User p as, $G_{\text{d}}=0.5$ and $G_{\text{c}}=\left(\alpha_p\alpha_q\gamma_{\text{th}}I_5\right)^{-2}$.

2) Asymptotic OP of User q:

Similarly, by applying (45) in (41), the asymptotic OP of User q can be written as

$$F_{\gamma_q}^{\infty}\left(\gamma_{\rm th}\right) \approx \alpha_q \frac{\gamma_{\rm th}\left(\gamma_{\rm th}+2\right)}{\bar{\gamma} Q_q}. \quad (50)$$

Based on (50) and (43), one can immediately find out the two performance metrics of User q as, $G_{\rm d}=1$ and $G_{\rm c}=\left[\alpha_q \gamma_{\rm th}\left(\gamma_{\rm th}+2\right)/Q_q\right]^{-1}$.

Interestingly, we find that the diversity order of User p is smaller than that of User q. This phenomenon can be explained by the fact that User p is served after the capacity requirement of User q is satisfied, and the SINR of User p is affected by the link quality of User q as shown in (10).

E. ASER

From [39], the ASER of wireless systems in terms of *M*-ary phase shift keying (*M*-PSK) modulation can be written as

$$P_{M-\rm PSK}^{j} = \frac{1}{\pi}\int_0^{\pi-\frac{\pi}{M}} M_{\gamma_j}\left(\frac{\sin^2\left(\pi/M\right)}{\sin^2\theta}\right) d\theta \quad (51)$$

where $M_{\gamma_j}\left(s\right)=\mathrm{E}\left[e^{-s\gamma_j}\right]$ is the moment generate function (MGF) of γ_j. Since the closed-form expression of (51) is intractable, we resort to [9] to approximate (51) as

$$P_{M-\rm PSK}^{j} \approx \left(\frac{\theta_M}{2\pi}-\frac{1}{4}\right) M_{\gamma_j}\left(\sin^2\left(\frac{\pi}{M}\right)\left(\sin^2\theta\right)^{-1}\right) + \frac{1}{4} M_{\gamma_j}\left(\frac{4}{3}\sin^2\left(\frac{\pi}{M}\right)\right) + \left(\frac{\theta_M}{2\pi}-\frac{1}{6}\right) M_{\gamma_j}\left(\sin^2\left(\frac{\pi}{M}\right)\right). \quad (52)$$

To analyze the ASER performance of NOMA users, we evaluate the MGFs of Users p and q as follows:

1) The MGF of User p:

From (10), the MGF of User p can be written as

$$M_{\gamma_p}\left(s\right) = \mathrm{E}\left[e^{-s\gamma_p}\right] = \int_0^{\infty}\underbrace{\int_0^{\infty} e^{-\frac{s\bar{\gamma}Q_p x}{\sqrt{1+\bar{\gamma}Q_q y}+1}} f_{|h_p|^2}\left(x\right) dx}_{I_6} f_{|h_q|^2}\left(y\right) dy. \quad (53)$$

Inserting (2) into (53) along with [28, (9.14.1), (3.381.4)], I_6 can be computed as

$$I_6 = \alpha_p \sum_{k=0}^{\infty} \frac{\left(m_p\right)_k \delta_p^k \Gamma\left(k+1\right)}{\left(k!\right)^2}\left(\frac{s\bar{\gamma}Q_p}{\sqrt{1+\bar{\gamma}Q_q y}+1}+\beta_p\right)^{-k-1}. \quad (54)$$

Substituting (2) and (54) into (53), along with binomial theorem, [31, (10)], and [32, (2.6.2)], $M_{\gamma_p}\left(s\right)$ can be obtained as (55) at the top of the next page with $w=k+1+v$.

2) The MGF of User q:

From (11), the MGF of User q can be computed as

$$M_{\gamma_q}\left(s\right) = \mathrm{E}\left[e^{-s\gamma_q}\right] = e^{s}\int_0^{\infty} e^{-s\sqrt{1+\bar{\gamma}Q_q y}} f_{|h_q|^2}\left(y\right) dy. \quad (56)$$

In order to compute the integral in (56), we first exploit $e^{-s\sqrt{1+\bar{\gamma}Q_q y}}$ in terms of series expressions according to [28, (1.211.1)]. Then, with the aid of [31, (10)], we obtain

$$e^{-s\sqrt{1+\bar{\gamma}Q_q y}} = \sum_{k=0}^{\infty}\frac{\left(-s\right)^k}{k!\Gamma\left(-\frac{k}{2}\right)} G_{1,1}^{1,1}\left[\bar{\gamma}Q_q y\,\middle|\,\begin{matrix}1+0.5k\\0\end{matrix}\right]. \quad (57)$$

TABLE I
SATELLITE CHANNEL PARAMETERS [27].

Shadowing	b_j	m_j	Ω_j
Heavy shadowing (HS)	0.063	0.739	8.97×10^{-4}
Average shadowing (AS)	0.126	10.1	0.835
Light shadowing (LS)	0.158	19.4	1.29

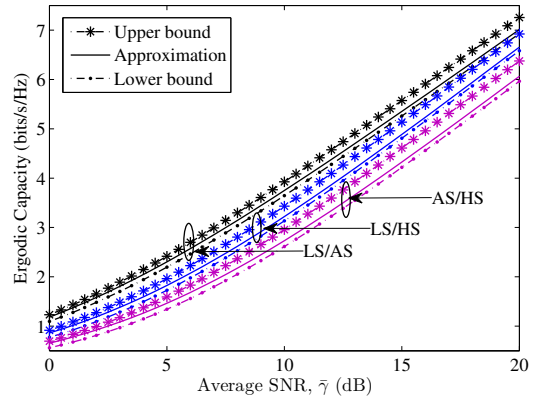

Fig. 2. The ergodic capacity versus the average SNR $\bar{\gamma}$ for various shadowing scenarios.

To this end, substituting (2), (19), and (57) into (56) along with the help of [32, (2.6.2)], we have

$$M_{\gamma_q}\left(s\right) = \frac{\alpha_q e^{s}}{\Gamma\left(m_q\right)}\sum_{k=0}^{\infty}\frac{\left(-s\right)^k}{k!\Gamma\left(-0.5k\right)} \times G_{1,[1:1],0,[1:2]}^{1,1,1,1,1}\left[\begin{matrix}\frac{\bar{\gamma}Q_q}{\beta_q}\\ \\ \frac{-\delta_q}{\beta_q}\end{matrix}\,\middle|\,\begin{matrix}1\\1+0.5k;1-m_q\\--\\0;0,0\end{matrix}\right]. \quad (58)$$

IV. NUMERICAL RESULTS

In this section, numerical results are provided to validate the theoretical analysis and show the superiority of the proposed NOMA-based strategy in the LMS network. Specifically, the channel parameters depending on the referred shadowing scenario for satellite links are given in Table I [27]. Moreover, we set the carrier frequency to be 1.6 GHz, $\varphi_p=0.1^{\circ}$, $\varphi_q=0.6^{\circ}$, $\varphi_{p3\rm dB}=\varphi_{q3\rm dB}=0.4^{\circ}$, and $G_p=G_q=3.5$ dBi, $G_s=24.3$ dBi, $\xi=2$, and $P_{\rm int}=50$ W [7], [40]. The label (LS/HS) denotes the link shadowing severity of User-*p*/User-*q*.

Fig. 2 depicts the approximation as well as the upper and lower bounds of the ergodic capacity versus $\bar{\gamma}$ for various shadowing effect of satellite links. As we clearly see, both the upper and lower bounds are tight and match well with the approximated curves across the entire $\bar{\gamma}$ range. In addition, we can see that a better ergodic capacity performance is achieved when User p or User q experiences a better quality of satellite link. This is an expected result since better links correspond to more favourable conditions.

The comparison of ergodic capacity between the NOMA and the TDMA schemes for different fading severities of satellite links is plotted in Fig. 3. As shown in the figure, for all cases, the ergodic capacity curves with the NOMA scheme are

$$M_{\gamma_p}(s) = \alpha_p \sum_{k=0}^{\infty}\sum_{v=0}^{\infty}\binom{-k-1}{v}\sum_{m=0}^{\infty}\binom{-v}{m}\frac{(m_p)_k \delta_p^k \Gamma(k+1)(s\bar{\gamma}Q_p)^v \beta_p^{-w}\alpha_q}{(k!)^2\Gamma(-0.5m)\Gamma(m_q)\beta_q} G^{1,1,1,1,1}_{1,[1:1],0,[1:2]}\left[\begin{array}{c|c} \frac{\bar{\gamma}Q_q}{\beta_q} & 1 \\ & 1+0.5m; 1-m_q \\ \frac{-\delta_q}{\beta_q} & -- \\ & 0,0;0 \end{array}\right]. \quad (55)$$

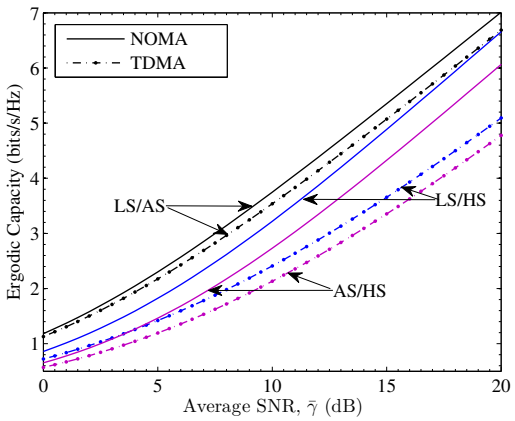

Fig. 3. The ergodic capacity versus the average SNR $\bar{\gamma}$ for different multiple access schemes.

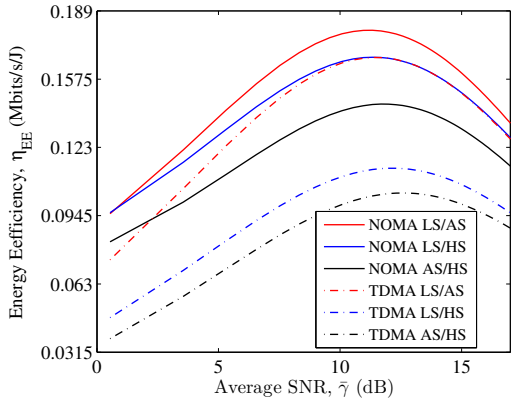

Fig. 4. EE η_{EE} versus the average SNR $\bar{\gamma}$ with various fading scenarios.

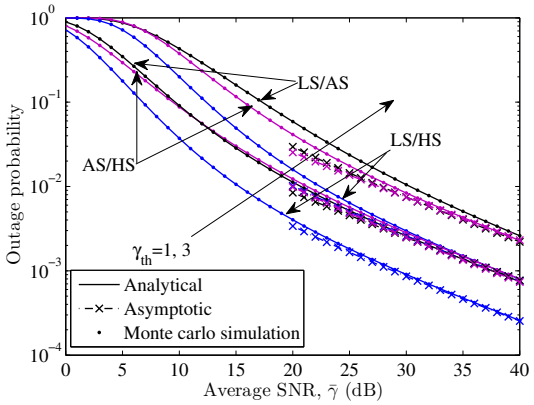

Fig. 5. The OP of User p versus the average SNR $\bar{\gamma}$ under different values of γ_{th} and shadowing configurations.

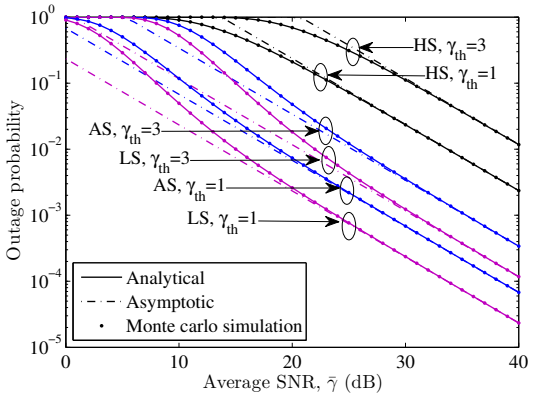

Fig. 6. The OP of User q versus the average SNR $\bar{\gamma}$ under various values of γ_{th} and fading configurations.

superior to those with the TDMA scheme, particularly at high $\bar{\gamma}$. The reason is that the NOMA scheme allows user to use all frequency/time resources, while the TDMA scheme only enables user to exploit frequency resource in limited time slots. Moreover, we note that the superiority of the NOMA scheme will be significantly degraded if the link quality of User q improves, i.e., the capacity gap between the NOMA and the TDMA in LS/AS is much smaller than that in LS/HS. This is due to the fact that α_2 gets smaller for a better propagation condition of User q, which in turn decreases the sum rate gap R_{gap} as analyzed in Section II. This observation is consistent with the statements made in [14] and [15], that the superiority of the NOMA scheme increases as the difference in channel gains between the NOMA users is larger.

Fig. 4 shows the EE of the NOMA and the TDMA schemes versus $\bar{\gamma}$ for different shadowing scenarios. It can be seen from Fig. 4 that for both multiple access schemes, EE curves first significantly increase and then at certain point decrease as $\bar{\gamma}$ increases. The point occurs at a little higher $\bar{\gamma}$ for a more serious shadowing propagation of User p or User q. Besides, for all cases, the EE of the two multiple access schemes improves when User p or User q experiences a better shadowing scenario. This is because a better shadowing propagation from the satellite to the destination is corresponding to higher ergodic capacity, which has been demonstrated in Fig. 2. Meanwhile, we can clearly find that the EE curves obtained through the NOMA schemes significantly outperform those of the TDMA schemes, since higher ergodic capacity can be achieved with the same amount of power consumption. This observation indicates that the LMS system employing the NOMA scheme can use the on-board energy more efficiently, which is beneficial for a limited energy resources (solar panel, battery pack), and can further provide an economic benefit because smaller launch vehicles may be chosen.

In Figs. 5 and 6, the OP performances of Users p and q are illustrated, respectively. As observed in those figures,

This article has been accepted for publication in a future issue of this journal, but has not been fully edited. Content may change prior to final publication. Citation information: DOI 10.1109/ACCESS.2018.2844783, IEEE Access

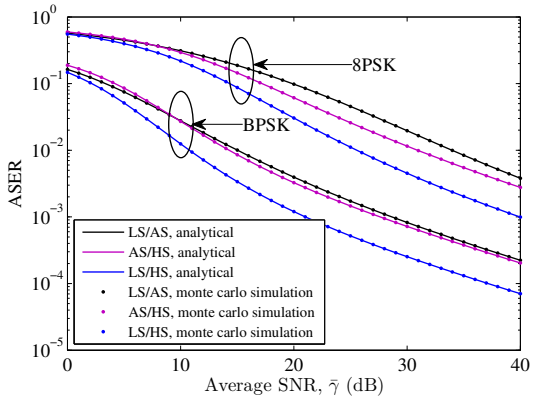

Fig. 7. The ASER of User p for different fading scenarios in terms of BPSK and 8PSK modulation schemes.

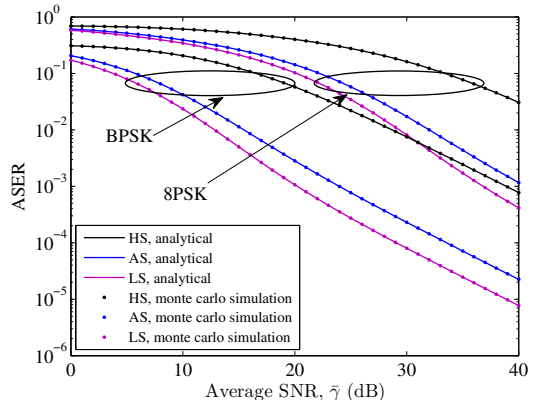

Fig. 8. The ASER of User q for various shadowing scenarios in terms of BPSK and 8PSK modulation schemes.

the analytical results computed by (33) and (35) agree well with the Monte Carlo simulations, implying that the theoretical analysis can accurately evaluate the OP performance. Meanwhile, the asymptotic curves calculated by (42) and (43) match well with the analytical curves at the high SNR regime. In addition, increasing the threshold $\gamma_{\rm th}$ from 1 to 3 dB, the OP performances of both User p and User q significantly degrade, which indicates the significant impact of the threshold $\gamma_{\rm th}$ on the OP performance. Interestingly, as shown in Fig. 5 and Fig. 6, different OP performance can be obtained for various fading configurations of User q, i.e., a heavier shadowing severity of User q obviously improves the OP performance of User p, but degrades the OP performance of User q at the same time, since γ_p given in (6) is increasing, while the γ_q given in (7) is decreasing. This phenomenon suggests that we should take into account the OP performance of the user with weaker channel gain when forming a NOMA group. In particular, by comparing those asymptotic OP curves in Figs. 5 and 6, we can see that User p and User q experience different diversity orders, which confirms the diversity order results evaluated in section III. Furthermore, the deterioration of shadowing severity does not impact the diversity order, but it does degrade the OP performance of NOMA users in terms of coding gain.

Figs. 7 and 8 present the ASER performances of User p and User q with M-PSK modulation, respectively. Similar to the case of the OP performance, a more severe shadowing link of User q can apparently improves the ASER performance of User p, but degrade that of User q.

V. CONCLUSION

In this paper, we have introduced the NOMA scheme in a LMS network and investigated the performance of the considered system. Specifically, theoretical expressions for ergodic capacity, EE, OP, asymptotic OP, and ASER performances have been derived. Simulations have been provided to validate those performance analyses and illustrate the effect of key parameters such as fading parameters and user selection strategy on the system performance. Our findings have demonstrated that the ergodic capacity and EE performances of the considered system can be significantly improved compared with the TDMA scheme, showing the benefits of applying the NOMA scheme to the LMS system. Moreover, when the channel link quality of heavier shadowing user becomes more serious, the ergodic capacity and EE performances of the considered system can be further improved, but the OP and ASER performances of the heavier shadowing user are degraded. This phenomenon indicates that we should take into account the superiority of the NOMA scheme and the QoS requirement of user with worse shadowing when forming a NOMA group.

REFERENCES

[1] S. K. Sharma, S. Chatzinotas, and B. Ottersten, "Satellite cognitive communications: interference modeling and techniques selection," in *Proc. 6th Advanced Satellite Multimedia Systems Conference (ASMS) and 12th Signal Processing for Space Communications Workshop (SPSC)*, Baiona, Spain, Sept. 2012, pp. 111-118.

[2] B. Li, Z. Fei, X. Xu, and Z. Chu, "Resource allocations for secure cognitive satellite-terrestrial networks," *IEEE Commun. Lett.*, in press.

[3] K. An, M. Lin, W.-P. Zhu, Y. Huang, and G. Zheng, "Outage performance of cognitive hybrid satellite–terrestrial networks with interference constraint," *IEEE Trans. Veh. Technol.*, vol. 65, no. 11, pp. 9397–9404, Nov. 2016.

[4] S. Vassaki, M. I. Poulakis, A. D. Panagopoulos, and P. Constantinou, "Power allocation in cognitive satellite terrestrial networks with QoS constraints," *IEEE Commun. Lett.*, vol. 17, no. 7, pp. 1344–1347, Jul. 2013.

[5] K. An, M. Lin, T. Liang, J. Ouyang, and W.-P. Zhu, "On the ergodic capacity of multiple antenna cognitive satellite terrestrial networks," in *Proc. IEEE ICC'16*, Kuala Lumpur, Malaysia, Jul. 2016.

[6] C. Yuan, M. Lin, J. Ouyang, and Y. Bu "Joint security beamforming in cognitive hybrid satellite-terrestrial networks," in *Proc. IEEE VTC'16*, Nanjing, China, May 2016.

[7] K. An, M. Lin, J. Ouyang, and W.-P. Zhu, "Secure transmission in cognitive satellite terrestrial networks," *IEEE J. Sel. Areas Commun.*, vol. 34, no. 11, pp. 3025–3037, Nov. 2016.

[8] B. Evans, M. Wemer, E. Lutz, M. Bousquet, G. E. Corazza, G. Maral, and R. Rumeau, "Integration of satellite and terrestrial systems in future media communications," *IEEE Wireless Commun.*, vol. 12, no. 5, pp. 72–80, Oct. 2005.

[9] M. R. Bhatnagar and M. K. Arti, "Performance analysis of AF based hybrid satellite-terrestrial cooperative network over generalized fading channels," *IEEE Commun. Lett.*, vol. 17, no. 10, pp. 1912–1915, Oct. 2013.

[10] M. K. Arti, "Channel estimation and detection in hybrid satellite-terrestrial communication systems," *IEEE Trans. Veh. Technol.*, vol. 65, no. 7, pp. 5764–5771, Jul. 2016.

[11] S. Sreng, B. Escrig, and M.-L. Boucheret, "Exact outage probability of a hybrid satellite terrestrial cooperative system with best relay selection," in *Proc. IEEE ICC'13*, Budapest, Hungary, Jun. 2013, pp. 4520–4524.

[12] L. Yang and M. O. Hasna, "Performance analysis of amplify-and-forward hybrid satellite-terrestrial networks with cochannel interference," *IEEE Trans. Commun.*, vol. 63, no. 12, pp. 5052–5061, Dec. 2015.
[13] K. Higuchi and A. Benjebbour, "Non-orthogonal multiple access (NOMA) with successive interference cancellation for future radio access," *IEICE Trans. on Commun.*, vol. E98-B, no. 3, pp. 403–414, Mar. 2015.
[14] Y. Saito, Y. Kishiyama, A. Benjebbour, T. Nakamura, and A. Li, K. Higuchi, "Non-orthogonal multiple access (NOMA) for cellular future radio access," in *Proc. VTC'13*, Dresden, Germany, Jun. 2013, pp. 1–5.
[15] L. Lv, Q. Li, Z. Ding, and J. Chen, "Application of non-orthogonal multiple access in cooperative spectrum-sharing networks over Nakagami-m fading channels," *IEEE Trans. Veh. Technol.*, vol. 66, no. 6, pp. 5506–5511, Jun. 2017.
[16] Z. Ma, Z. Zhang, Z. Ding, P. Fan, and H. Li, "Key techniques for 5G wireless communications: network architecture, physical layer, and MAC layer perspectives," *Sci. China Inf. Sci*, vol. 58, no. 4, pp. 1–20, Apr. 2015.
[17] Z. Yang, Z. Ding, P. Fan, and Z. Ma, "Outage performance for dynamic power allocation in hybrid non-orthogonal multiple Aaccess systems," *IEEE Commun. Lett.*, vol. 20, no. 8, pp. 1695–1698, Aug. 2016.
[18] X. Li, C. Li, and Y. Jin, "Dynamic resource allocation for transmit power minimization in OFDM-based NOMA systems," *IEEE Commun. Lett.*, vol. 20, no. 12, pp. 2558–2561, Dec. 2016.
[19] Z. Yang, Z. Ding, P. Fan, and N. Al-Dhahir, "A general power allocation scheme to guarantee quality of service in downlink and uplink NOMA systems," *IEEE Trans. Wireless Commun.*, vol. 15, no. 11, pp. 7244–7257, Nov. 2016.
[20] X. Zhang, Q. Gao, C. Gong, and Z. Xu, "User grouping and power allocation for NOMA visible light communication multi-cell networks," *IEEE Commun. Lett.*, vol. 21, no. 4, pp. 777–780, Apr. 2017.
[21] X. Zhu, C. Jiang, L. Kuang, N. Ge, and J. Lu, "Non-orthogonal multiple access based integrated terrestrial-satellite networks," *IEEE J. Sel. Areas Commun.*, vol. 35, no. 10, pp. 2253–2267, Oct. 2017.
[22] X. Yan, H. Xiao, C.-X. Wang, and K. An, "Outage performance of NOMA-based hybrid satellite-terrestrial relay networks," *IEEE Wireless Commun. Lett.*, in press.
[23] X. Yan, H. Xiao, K. An, G. Zhen, and W. Tao, "Hybrid satellite terrestrial relay networks with cooperative non-orthogonal multiple access," *IEEE Commun. Lett.*, in press.
[24] M. Zeng, A. Yadav, O. A. Dobre, G. I. Tsiropoulos, and H. V. Poor, "Capacity comparison between MIMO-NOMA and MIMO-OMA with multiple users in a cluster," *IEEE J. Sel. Areas Commun.*, vol. 35, no. 10, pp. 2413–2424, Oct. 2017.
[25] M. K. Arti, "Channel estimation and detection in satellite communication systems," *IEEE Trans. Veh. Technol.*, vol. 65, no. 12, pp. 10173-10179, Dec. 2016.
[26] G. Zheng, S. Chatzinotas and B. Ottersten, "Generic optimization of linear precoding in multibeam satellite systems," *IEEE Trans. Wireless Commun.*, vol. 11, no. 6, pp. 2308–2320, Jun. 2012.
[27] A. Abdi, W. Lau, M.-S. Alouini, and M. Kaveh, "A new simple model for land mobile satellite channels: first and second order statistics," *IEEE Trans. Wireless. Commun.*, vol. 2, no. 3, pp. 519–528, May 2003.
[28] I. S. Gradshteyn and I. M. Ryzhik, *Table of Integrals, Series, and Products*, 7th ed. New York, NY, USA: Academic, 2007.
[29] M. Caus, M. A. Vazquez, and A. Perez-Neira, "NOMA and interference limited satellite scenarios." in *Proc. IEEE ACSSC'16*, Pacific Grove, CA, USA, Mar. 2017, pp. 497–501.
[30] D. B. da Costa and S. Aissa, "Capacity analysis of cooperative systems with relay selection in nakagami-m fading," *IEEE Commun. Lett.*, vol. 13, no. 9, pp. 637–640, Sep. 2009.
[31] V. S. Adamchik and O. I. Marichev, "The algorithm for calculating integrals of hypergeometric type functions and its realization in reduce systems," in *Proc. ISSAC'90*, Tokyo, Japan, Aug. 1990, pp. 212–224.
[32] A. M. Mathai and R. K. Saxena, *The H-function with applications in statistics and other disciplines*, New York, NY, USA:Wiley, 1978.
[33] R. P. Agrawal, "On certain transformation formulae and Meijer's G-function of two variables," *Indian J. Pure Appl. Math.*, vol. 1, no. 4, pp. 537–551, Mar. 1970.
[34] I. S. Ansari, S. Al-Ahmadi, F. Yilmaz, M.-S. Alouini, and H. Yanikomeroglu, "A new formula for the BER of binary modulations with dual-branch selection over generalized-K composite fading channels," *IEEE Trans. Commun.*, vol. 59, no. 10, pp. 2654–2658, Oct. 2011.
[35] Y. Huang, F. Al-Qahtani, C. Zhong, Q. Wu, J. Wang, and H. Alnuweiri, "Performance analysis of multiuser multiple antenna relaying networks with co-channel interference and feedback delay," *IEEE Trans. Commun.*, vol. 62, no. 1, pp. 59–73, Jan. 2014.
[36] P. Patcharamaneepakorn, S. Wu, C.-X. Wang, e.-H. M. Aggoune, M.-M. Alwakeel, X. Ge, and M. D. Renzo, "Spectral, energy, and economic efficiency of 5G multicell massive MIMO systems with generalized spatial modulation," *IEEE Trans. Veh. Technol.*, vol. 65, no. 12, pp. 9715–9731, Feb. 2016.
[37] V. K. Sakarellos and A. D. Panagopoulos, "Outage performance of cooperative land mobile satellite broadcasting systems," in *Proc. Eur. Conf. Antennas Propag.*, Gothenburg, Sweden, Apr. 2013, pp. 473–476.
[38] Z. Wang and G. Giannakis, "A simple and general parameterization quantifying performance in fading channels," *IEEE Trans. Commun.*, vol. 51, no. 8, pp. 1389–1398, Aug. 2003.
[39] M. K. Simon and M. S. Alouini, *Digital Communication over Fading Channels: A Unified Approach to Performance Analysis*, Hoboken, NJ, USA: Wiley, 2000.
[40] A. Kalantari, G. Zheng, Z. Gao, Z. Han, and B. Ottersten, "Secrecy analysis on network coding in bidirectional multibeam satellite communications," *IEEE Trans. Inf. Forensics Security*, vol. 10, no. 9, pp. 1862-1874, Sep. 2015.

APPENDIX A
DERIVATION THE RANGE OF α

During the same time slots, the capacity of Users p and q with the TDMA scheme can be respectively calculated as

$$R_p^{\mathrm{TDMA}} = 0.5\log_2\left(1+\bar{\gamma}Q_p\left|h_p\right|^2\right) \tag{59}$$

and

$$R_q^{\mathrm{TDMA}} = 0.5\log_2\left(1+\bar{\gamma}Q_q\left|h_q\right|^2\right). \tag{60}$$

Assuming the capacity achieved by User p with the NOMA scheme is better than that with the TDMA scheme, we have

$$\begin{aligned}&\log_2\left(1+\alpha\bar{\gamma}Q_p\left|h_p\right|^2\right) \geq 0.5\log_2\left(1+\bar{\gamma}Q_p\left|h_p\right|^2\right)\\ &\Rightarrow \alpha\bar{\gamma}Q_p\left|h_p\right|^2 \geq \sqrt{1+\bar{\gamma}Q_p\left|h_p\right|^2}-1\\ &\Rightarrow \alpha \geq 1\Big/\left(\sqrt{1+\bar{\gamma}Q_p\left|h_p\right|^2}+1\right).\end{aligned} \tag{61}$$

Similarly, assuming the capacity achieved by User q with the NOMA scheme is better than that with the TDMA scheme, we get

$$\begin{aligned}&\log_2\left(1+\tfrac{(1-\alpha)\bar{\gamma}Q_q|h_q|^2}{\alpha\bar{\gamma}Q_q|h_q|^2+1}\right) \geq 0.5\log_2\left(1+\bar{\gamma}Q_q\left|h_q\right|^2\right)\\ &\Rightarrow \alpha\bar{\gamma}Q_q|h_q|^2\sqrt{1+\bar{\gamma}Q_q|h_q|^2} \leq \bar{\gamma}Q_q|h_q|^2-\sqrt{1+\bar{\gamma}Q_q|h_q|^2}+1\\ &\Rightarrow \alpha \leq 1\Big/\left(\sqrt{1+\bar{\gamma}Q_q\left|h_q\right|^2}+1\right).\end{aligned} \tag{62}$$

Finally, defining $\alpha_1=\frac{1}{\sqrt{1+\bar{\gamma}Q_p|h_p|^2}+1}$ and $\alpha_2=\frac{1}{\sqrt{1+\bar{\gamma}Q_q|h_q|^2}+1}$, we obtain the desired range of α shown in (9).